# Analysis and Correction of Dual PRF Velocity Data

IWAN HOLLEMAN AND HANS BEEKHUIS

*Royal Netherlands Meteorological Institute (KNMI), De Bilt, Netherlands*

(Manuscript received 23 January 2002, in final form 12 September 2002)

ABSTRACT

The dual pulse repetition frequency (dual PRF) technique for extension of the unambiguous velocity interval is available on many operational Doppler weather radars. Radial velocity data obtained from a C-band Doppler radar running in dual PRF mode have been analyzed quantitatively. The standard deviation of the velocity estimates and the fraction of dealiasing errors are extracted and related using a simple model. A postprocessing algorithm for dual PRF velocity data, which removes noise and corrects dealiasing errors, has been developed and tested. It is concluded that the algorithm is very efficient and produces high quality velocity data.

## 1. Introduction

Doppler weather radars are capable of providing high quality wind data at a high spatial and temporal resolution. This kind of data is of great value for operational weather forecasting and numerical weather prediction (NWP) models. Doppler velocity information can be used for removal of ground clutter, extraction of wind profiles, detection of shear zones, and construction of dual Doppler wind fields (Meischner et al. 1997; Serafin and Wilson 2000; Chong et al. 2000). In addition, the radial velocity data and wind profiles can be assimilated into NWP models (Collins 2001; Lindskog et al. 2000). Operational application of Doppler velocity data from weather radars is hampered, however, by the infamous limitation of the range–velocity ambiguity. This is particularly true for a C-band weather radar, since its ambiguity limitation is a factor of 2 more stringent than that of an S-band radar. Aliased velocity data from S-band radars can be unfolded using local continuity in one or more dimensions and environmental constraints (Hennington 1981; Merritt 1984; Desrochers 1989; Bergen and Albers 1988; Eilts and Smith 1990). Eilts and Smith (1990) have found that velocity data of acceptable quality are obtained for these radars provided that the wind shear is not extreme. Due to the smaller unambiguous velocity interval, this kind of approach is not feasible for C-band radars without relying heavily on external wind profiles (Hondl and Eilts 1993). To this day, Doppler velocity data from the operational C-band weather radars in Europe are mainly used for removal of ground clutter and extraction of wind profiles (Meischner et al. 1997).

Doviak and Sirmans (1973) have proposed to extend the unambiguous velocity by transmission of orthogonally polarized waves in pairs of pulses. This pulse diversity technique has successfully been employed by a mobile W-band radar for velocity measurements in tornadoes (Bluestein and Pazmany 2000). The use of two interlaced sampling rates for the extension of the unambiguous velocity of single polarization radars has been introduced by Sirmans et al. (1976). The application of this staggered pulse repetition time (PRT) technique is hampered thus far by the inability of most operational weather radars to run in staggered PRT mode and associated problems with filtering of ground clutter. To tackle the latter problem, Sachidananda and Zrnić (2000) have presented a new processing algorithm based on Fourier transform and magnitude deconvolution. Dazhang et al. (1984) have put forward a method wherein velocity estimates are made using two alternating pulse repetition frequencies (PRFs), that is, employing $M_1$ pulses at one PRF followed by $M_2$ pulses at the other PRF. This dual PRF technique allows for straightforward filtering of ground clutter and an extension of the unambiguous velocity interval. The dual PRF technique is available on a large part of the operational C-band Doppler weather radars, but it is not used widely as of yet.

Recently, the interest in the dual PRF technique for extending the unambiguous velocity interval of C-band and X-band radars has increased. Hildebrand et al. (1996) have developed the electra Doppler radar (ELDORA), which is an airborne X-band radar with dual PRF capability. Detailed cross sections through severe thunderstorms and tornadoes have been recorded with this radar and unfolded velocities of more than 80 m

*Corresponding author address:* Dr. Iwan Holleman, Royal Netherlands Meteorological Institute (KNMI), P.O. Box 201, NL AE 3730 De Bilt, Netherlands.
E-mail: holleman@knmi.nl

$s^{-1}$ have been observed. Jorgensen et al. (2000) present examples of raw dual PRF velocity data from another X-band airborne Doppler radar and discuss the cause of the dealiasing errors. The effect of azimuthal shear of the radial wind on the quality of dual PRF data has been investigated by May (2001) using a mesocyclone model. May and Joe (2001) have presented an algorithm for correcting dealiasing errors in dual PRF velocity data.

In this article we present an extended analysis of dual PRF velocity data and a three-step postprocessing algorithm for correction of the data. First, a short introduction to the dual PRF technique and a description of the available radar data are given. Then, qualitative and quantitative characteristics of dual PRF data are elucidated via different analyzes of measured velocity fields. These analyzes confirm that the velocity outliers, which are characteristic for dual PRF data, are in fact isolated dealiasing errors. Finally, a three-step algorithm for the correction of dual PRF velocity data is described in detail. The processing algorithm is intended for operational use, and preliminary results indicate that the quality of the velocity fields is enhanced significantly and that further use of the data has become feasible.

## 2. Dual PRF technique

The operational application of Doppler weather radar, especially C band or shorter wavelengths, has been hampered by the small unambiguous velocity interval of the instrument. The unambiguous or Nyquist velocity of a Doppler radar using uniformly spaced pulses is given by (Doviak and Zrnić 1993)

$$V_i^u = \frac{\lambda \mathrm{PRF}_i}{4}, \tag{1}$$

where $\lambda$ is the wavelength used by the radar, and $\mathrm{PRF}_i$ is the pulse repetition frequency. The PRF also determines the unambiguous range of the radar. The unambiguous velocity and range of a Doppler radar are coupled, and a trade-off has to be made. The product of the unambiguous velocity and range is given by (Doviak and Zrnić 1993)

$$V_i^u R_i^u = \frac{c\lambda}{8}, \tag{2}$$

where $c$ is the speed of light. For a typical C-band ($\lambda = 5.3$ cm) radar, this product is roughly equal to 2000 km m $s^{-1}$. At a moderate range of 200 km, the unambiguous velocity is only 10 m $s^{-1}$. Velocities higher than the unambiguous one will be folded into the unambiguous interval.

Dazhang et al. (1984) have proposed to extend the maximum unambiguous Doppler velocity by use of two alternating pulse repetition frequencies. From Eq. (1), it is clear that the use of different PRFs results in different unambiguous velocities. The folding of a measured velocity will, therefore, be different for the two pulse repetition frequencies. By combining the velocity measurements at the two different PRFs, the unambiguous velocity interval can be extended. Using a high and a low PRF with unambiguous velocities of $V_h^u$ and $V_l^u$, respectively, the extended unambiguous velocity becomes (Dazhang et al. 1984)

$$V_{lh}^u = \frac{V_h^u V_l^u}{V_h^u - V_l^u}. \tag{3}$$

It is evident from this equation that the unambiguous velocity interval is extended significantly when the high and low unambiguous velocities are close. It is common practice to choose the high and low PRFs such that the two unambiguous velocities are related in the following way:

$$\frac{V_h^u}{V_l^u} = \frac{\mathrm{PRF}_h}{\mathrm{PRF}_l} = \frac{N+1}{N}, \tag{4}$$

where the integer $N$ is the dual PRF unfolding factor. By insertion of Eq. (4) into Eq. (3), it can be verified that $N$ is indeed the factor by which the unambiguous velocity is extended with respect to $V_h^u$. With typical applications of the dual PRF technique, an unfolding factor $N$ of 2, 3, or 4 is used. It will be detailed below that for higher unfolding factors the quality of the measured velocities will be too poor.

A Doppler radar generally determines the radial velocity of the scatterers by autocorrelation of the received signal for subsequent transmitted pulses. During pulse-pair processing, the velocity is effectively deduced from the phase jump of the received signal between two subsequent pulses. The difference between the phase jump observed using the low PRF and that observed using the high PRF is employed by the dual PRF technique to deduce the radial velocity. Because the velocity is directly related to the observed phase difference or jump, the primary dual-PRF velocity estimate can be expressed in terms of the original velocities only:

$$\tilde{V}_{lh} = (N+1)\tilde{V}_l - N\tilde{V}_h, \tag{5}$$

where $\tilde{V}_h$ and $\tilde{V}_l$ are the observed velocities using the high and low PRF, respectively. When a velocity estimate falls outside of its unambiguous velocity interval, as given by Eq. (3), it should be folded back into the fundamental interval by addition or subtraction of $2V_{lh}^u$.

The primary dual PRF velocity estimate is obtained by the differencing of two phase measurements, and therefore, its standard deviation will be amplified. Using Eq. (5) and assuming that the errors in the high and low PRF velocities are uncorrelated, the standard deviation of the primary dual PRF velocity estimate becomes

$$\sigma_{lh} = \sqrt{(N+1)^2\sigma_l^2 + N^2\sigma_h^2} \tag{6}$$

$$\simeq \overline{\sigma}\sqrt{(N+1)^2 + N^2}, \tag{7}$$

where $\sigma_h$ and $\sigma_l$ are the standard deviations of the high and low PRF velocities, respectively. For large signal-

TABLE 1. Amplification of the std dev of the primary dual PRF velocity estimate with respect to that of the original–dealiased velocity as a function of the unfolding factor *N*.

| $N$ | 2 | 3 | 4 | 5 |
|---|---|---|---|---|
| $\sigma_{lh}/\overline{\sigma}$ | 3.6 | 5.0 | 6.4 | 7.8 |

to-noise ratios and narrow spectrum widths, the velocity standard deviation depends only on the wavelength, spectral width, and acquisition time, that is, the product of the number of transmitted pulses and their time spacing (Doviak and Zrnić 1993). The standard deviations of the high and low PRF velocities can be replaced by a single standard deviation $\overline{\sigma}$ when the acquisition times are equal. In Table 1, the calculated amplification of the standard deviation of the dual PRF velocity with respect to $\overline{\sigma}$ is given for relevant unfolding factors. It is evident that the standard deviation of the dual PRF velocity estimate increases rapidly with increasing unfolding factor.

In practice, the primary dual-PRF velocity estimate is not a suitable velocity estimator because of the large standard deviation (Sirmans et al. 1976; Dazhang et al. 1984; SIGMET 1998). The primary dual PRF velocity estimate is merely used to indicate to which Nyquist interval the original (folded) velocity estimates belong. In this way, unfolded velocity estimates are obtained with the standard deviation of the original velocities. This procedure introduces a type of errors in the velocity estimates that is distinctive for the dual PRF retrieval technique. Occasionally, the deviation of the primary dual PRF velocity estimate will be so large that the original folded velocity will be assigned to an incorrect Nyquist interval. This will give rise to clear outliers in the dual PRF velocity data. In section 4, the origin and characteristics of these outliers will be discussed in more detail.

## 3. Available radar data

The Royal Netherlands Meteorological Institute (KNMI) operates two identical C-band Doppler weather radars. In this study only data from the radar in De Bilt have been used. This radar is located at a latitude of 52.10°N and a longitude of 5.17°E and mounted at a height of 44 m above mean sea level. The Gematronik radar (Meteor AC360) has an antenna with a 4.2-m diameter and a beamwidth of about 1°. The transmitted pulses are generated by a magnetron and thus have random phases. The peak power and width of the transmitted pulses are 250 kW and 0.5 $\mu$s, respectively.

The returned signal is transferred to an analog receiver and subsequently digested by a Sigmet radar processor (RVP6). The radial velocity and spectral width are extracted from the received in-phase and quadrature-phase components using pulse-pair processing. Prior to the pulse-pair processing, ground clutter has been removed from the signal by an infinite impulse response filter in the time domain. The data are averaged to 0.5 km and 1° in range and azimuth, respectively. The collection of averaged data points as a function of range at a certain azimuth is denoted a ''ray.'' In dual PRF mode, the primary velocity is obtained by combining data from the actual ray with that from the previous ray. Subsequently, the velocity data from the actual ray are unfolded using the primary velocity estimate. The dual PRF unfolding is completely handled by the radar processor (SIGMET 1998). The data acquisition and generation of products are performed using the Rainbow software package of Gematronik. In dual PRF mode, the radar processor labels each ray with ''high'' or ''low'' according to the PRF used during acquisition. Unfortunately, Rainbow does not transfer these labels yet, but a workaround will be presented in a later section.

The operational scanning scheme of the radar, which consists of a 4-elevation volume scan every 5 min and a 14-elevation volume scan every 15 min, still has some gaps. These gaps have been used to perform a dedicated Doppler scan, which is repeated every 15 min. This scan is recorded at an elevation of 0.5° and an azimuthal speed of 4 rpm. The high PRF of 1000 Hz results in an unambiguous velocity of $V_h^u = 13.3$ m s$^{-1}$, and the low PRF of 750 Hz in $V_l^u = 10.0$ m s$^{-1}$. The extended unambiguous velocity interval of the dual PRF data thus becomes $V_{lh}^u = 39.9$ m s$^{-1}$.

For both the analysis of dual PRF velocity data and the testing of the correction algorithm, a set of about 300 different azimuthal Doppler scans is used. The scans have been recorded between 26 October and 30 November 2001. Only scans containing more than 10 000 valid data points, that is, about 10% of the total, and recorded on the hour, have been selected. In this period about 12 depressions moved from the North Atlantic into Scandinavia, while the associated frontal systems crossed the Netherlands. Mostly the frontal rain was followed by showers in polar or arctic air. In particular, the cold fronts and the showers produced significant weather with rain, snow, thunder, hail, and severe wind gusts. Strong gusts with wind speeds over 25 m s$^{-1}$ have been observed at the surface on 6 days, and the highest observed wind gust was up to 35 m s$^{-1}$. Wind speed data at 850 hPa, the altitude of the radar beam at 100-km range, from upper-air soundings at De Bilt have been analyzed. Between 26 October and 30 November 2001, the average and maximum wind speeds were 12 and 28 m s$^{-1}$, respectively. On 20 days within this period the observed wind speed was higher than the unambiguous velocity of the high PRF measurement, $V_h^u = 13.3$ m s$^{-1}$.

## 4. Analysis of dual PRF data

To elucidate the error characteristics of dual PRF velocity data, an analysis of measured velocity data has been performed. Figure 1 shows a typical example of

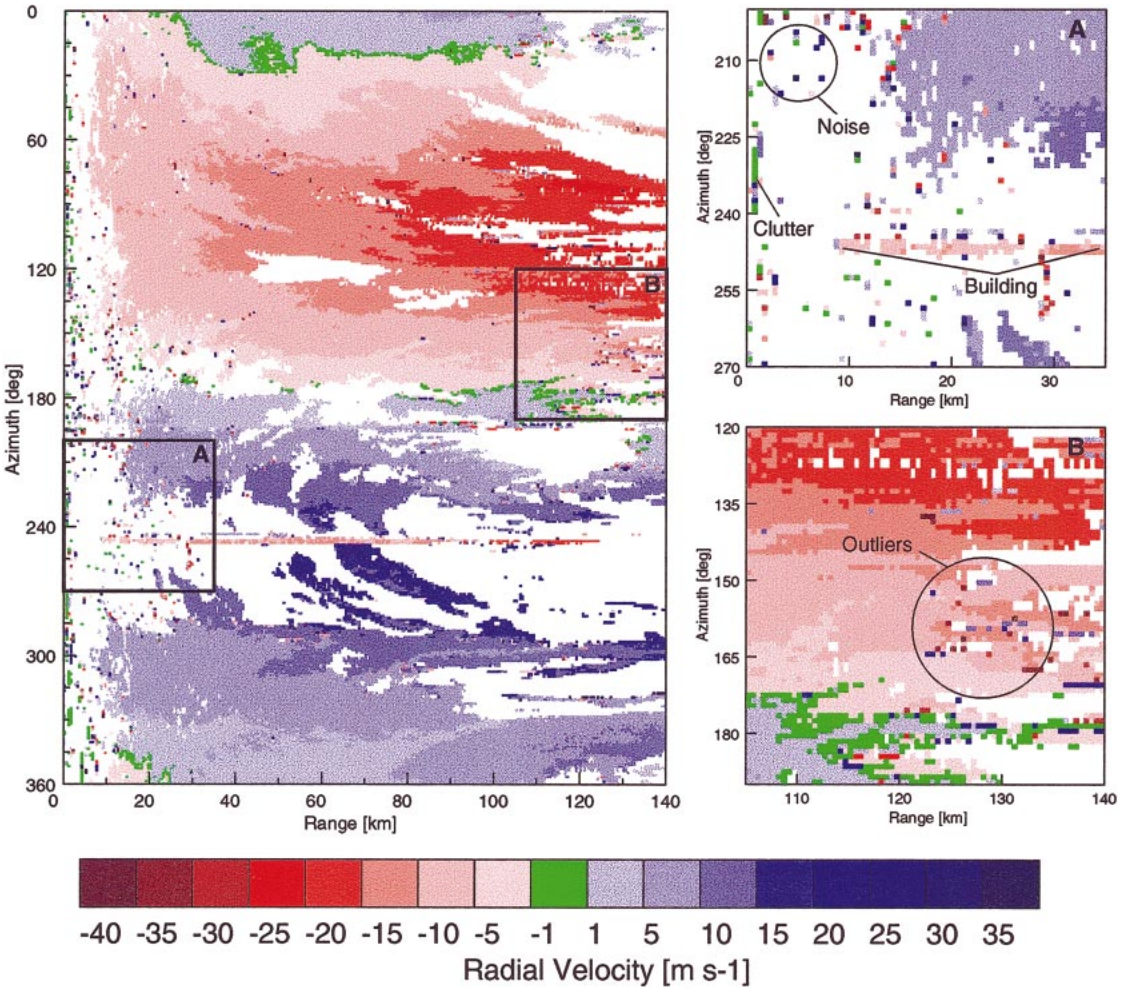


FIG. 1. B-scope display of raw dual PRF velocity data from 1454 UTC 6 Nov 2001. The azimuthal scan was recorded at an elevation of 0.5° using PRFs of 750 and 1000 Hz. Areas A and B of the main figure have been enlarged in the two frames on the right. Several sources of contamination have been marked in the figure. White indicates areas with ''missing data.''

raw dual PRF velocity data. This azimuthal scan has been recorded while a cold front was moving from west to east across the Netherlands. The cold front produced rainfall totals around 10 mm and maximum wind gusts of 21 m $s^{-1}$. The velocity data are presented in a so-called B-scope display or range–azimuth indicator, and two regions of interest have been enlarged in the right frames. From a close examination of Fig. 1 and other data, it appears that dual PRF velocity data are typically contaminated by clutter, noise, and outliers. These sources of contamination have been indicated in the side frames of Fig. 1. There is some sidelobe clutter present at ranges shorter than 10 km in Fig. 1, but the most distinct clutter is caused by specular reflection of the radar beam from a building located at 246° azimuth (see upper-right frame of Fig. 1). Noise from incidental scatterers is predominantly visible at short range (<35 km) because the echoes from nearby targets are very strong. The presence of velocity outliers in large areas of high quality data is characteristic for data obtained using the dual PRF technique. These dual PRF velocity outliers have been predicted and observed by others (Sirmans et al. 1976; Dazhang et al. 1984; Jorgensen et al. 2000; May and Joe 2001). Large areas with falsely dealiased velocities, which are characteristic for single PRF data, are not present in dual PRF data provided that the maximum velocity is below the dual PRF unambiguous velocity.

A quantitative analysis has been performed to obtain detailed information on the quality and outliers of dual PRF velocity data. For this, each velocity data point in an azimuthal scan is compared with the local median velocity. The local median velocity is calculated from the data point itself and the surrounding data points. An area measuring five range times three azimuth points is taken, and it is required that at least 9 out of the 15 data points contain valid data. The deviation of the data points from the local median values has been analyzed. In Fig. 2, histograms of the velocity deviations observed in the azimuthal scan of Fig. 1 are shown. For a reason

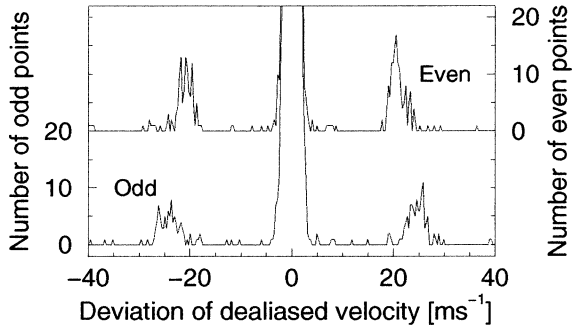


FIG. 2. Histogram of the deviations of each dealiased velocity from the local median velocity. This histogram has been compiled using the data of the azimuthal scan of Fig. 1. Separate histograms are shown for even and odd azimuths. The central peaks go up to a number of about 12 500 (off scale).

that will become clear, velocity data from even and odd azimuths have been collected into different histograms. The histograms have been constructed using a velocity bin size of 0.3 m s$^{-1}$ matching that of the dual PRF velocity data.

The central peaks of Fig. 2, containing the points with hardly any deviation from the local median velocity, go up to a number of about 12 500. The vast majority of the analyzed points obeys local continuity. The width of the central peaks is determined by the variance of the velocity data. A standard deviation of 0.50 and 0.49 m s$^{-1}$ is obtained for the even and odd azimuths, respectively. Equality of these standard deviations is expected, because the acquisition times for the high and low PRF measurements are equal [see Eq. (7)]. Apart from the central peak, two distinct sideband peaks are evident in both histograms of Fig. 2. The sideband peaks correspond to the velocity outliers, which are characteristic for the dual PRF technique. The number of points within the sidebands can be used to calculate the fraction of velocity outliers. The fraction of outliers is $9.1 \times 10^{-3}$ and $7.3 \times 10^{-3}$ for the even and odd azimuths, respectively. It is evident from Fig. 2 that the sidebands for even and odd azimuths are centered at different velocity deviations. The median deviation of the even azimuth sidebands is 20.9 m s$^{-1}$ and that of the odd azimuth sidebands is 24.6 m s$^{-1}$. These velocity deviations roughly match the unambiguous intervals of the low PRF (20.0 m s$^{-1}$) and high PRF (26.6 m s$^{-1}$) measurements. It is, therefore, concluded in accordance with others (Dazhang et al. 1984; Jorgensen et al. 2000; May and Joe 2001) that the velocity outliers in dual PRF data are caused by dealiasing errors. In addition, the observed sideband positions of the even and odd azimuths can be used to assign the proper PRF (high or low) to each ray.

The standard deviation of a Doppler velocity measurement depends on the actual meteorological circumstances. By combining the dual PRF velocity estimates with the spectral width data, this dependence can be demonstrated. For this, each velocity data point is again

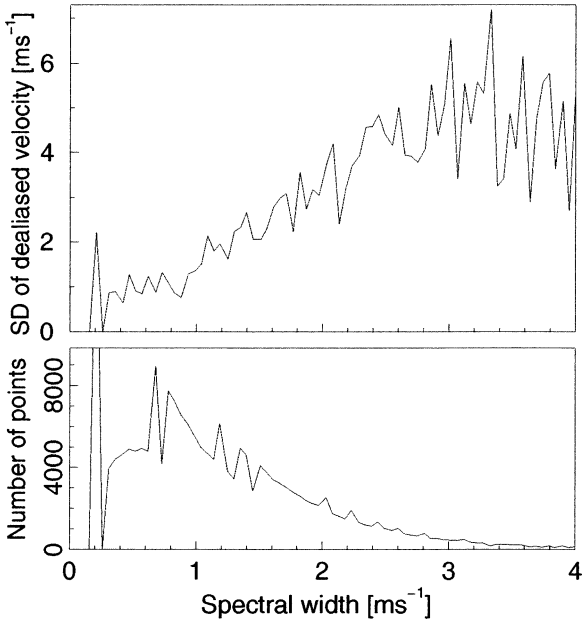


FIG. 3. (top) The std dev of the dealiased velocities is shown as a function of the spectral width; (bottom) the number of data points per spectral width bin ($\simeq$0.1 m s$^{-1}$) is shown. This figure has been put together using the velocity data from Fig. 1 and the corresponding spectral width data.

compared with the local median velocity. The standard deviation as a function of the spectral width is calculated by squaring the observed velocity deviations and summing them in different bins depending on the corresponding spectral width. The bin size is determined by the resolution of the available spectral width data and is equal to 0.1 m s$^{-1}$. By allowing a maximum velocity deviation of 11.6 m s$^{-1}$, equal to the average unambiguous velocity, possible outliers have been rejected. The upper frame of Fig. 3 shows the standard deviation as a function of spectral width as obtained from the azimuthal scan shown in Fig. 1 and the corresponding spectral width data. The number of data points per spectral width bin is shown in the lower frame of the figure. It is evident from Fig. 3 that the standard deviation depends strongly on the spectral width which is, among other things, affected by wind shear and turbulence (Doviak and Zrnić 1993). The flattening of the curve for larger spectral widths ($>$3 m s$^{-1}$) is an artifact caused by a decreasing number of data points and limitations of the method for calculation of the standard deviation. The excessive number of data points having a spectral width of 0.2 m s$^{-1}$ seems unrealistic, and is probably caused by a shortcoming in the radar processor or Rainbow software. Although the overall trend of the standard deviation in Fig. 3 compares favorably to calculations by Doviak and Zrnić (1993), a quantitative comparison is hampered by lack of information on, for instance, the signal-to-noise ratio.

Because the dual PRF dealiasing is completely handled by the radar processor, the primary dual PRF ve-

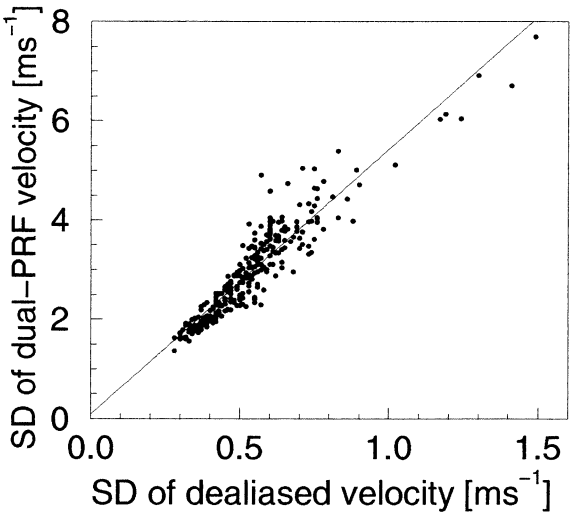


FIG. 4. Std dev of the primary dual PRF velocity estimates as a function of the std dev of the original–dealiased velocities for the set of 300 azimuthal scans (see section 3). The solid line with an intercept and slope of $0.1 \pm 0.1$ m s$^{-1}$ and $5.3 \pm 0.2$, respectively, is determined using linear regression.

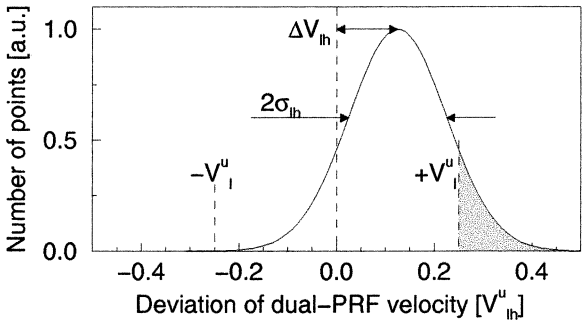


FIG. 5. Scheme illustrating the origin of the dealiasing errors in velocity data obtained using the dual PRF technique. The distribution of deviations of the primary velocity estimates is depicted. The parameters influencing this distribution, that is, std dev and bias, are indicated. The unambiguous velocity interval of the low PRF measurement for $N = 3$ unfolding has been indicated in the figure as well. The fraction of incorrectly dealiased data points is marked by the shaded area.

locity estimates are not available for further analysis. The primary dual PRF velocity estimates can, however, be reconstructed to a large extent from the dealiased data. For this, it is crucial that for each ray, it is known whether high or low PRF has been used during acquisition. When this information is not available, as in our case, it has to be deduced from the outlier analysis as presented in Fig. 2. The first step in the reconstruction is to fold the dealiased velocities back to their original fundamental Nyquist interval by adding or subtracting a multiple of $2V_h^u$ or $2V_l^u$ for high or low PRF, respectively. Subsequently, the primary dual PRF velocity estimate can be calculated for each valid data point using Eq. (5) when valid data are present in the same range bin of the previous ray as well. Using the method described previously, the standard deviation of the reconstructed, primary dual PRF velocity estimates can be calculated.

In Fig. 4, the standard deviation of the primary dual PRF velocities is plotted as a function of the standard deviation of the corresponding dealiased velocities using the set of 300 azimuthal scans (see section 3). A high correlation between the standard deviation of the primary dual PRF velocities and that of the dealiased velocities is evident from Fig. 4. The line determined using linear regression is shown in the figure as well. The resulting intercept and slope are $0.1 \pm 0.1$ m s$^{-1}$ and $5.3 \pm 0.2$, respectively. Thus, the standard deviation is about 5 times as large as that of the dealiased/original velocities, which is in almost perfect agreement with the theoretical ratio for $N = 3$ unfolding [see Eq. (7) and Table 1].

The large standard deviation of the primary velocity estimate is, together with possible azimuthal shear of the radial wind, the main cause of dealiasing errors (outliers) in dual PRF velocity data (Dazhang et al. 1984; May 2001). The origin of the dealiasing errors has been depicted schematically in Fig. 5. On the horizontal axis, the deviation of the primary velocity estimate relative to its unambiguous value is given. The Gaussian curve represents the distribution of possible deviations of the primary velocities, as implied by its standard deviation ($\sigma_{lh}$). The dual PRF technique employing data of the current and previous ray neglects azimuthal shear of the radial wind, that is, differences of true radial velocities in both rays. By insertion of a velocity difference in Eq. (5), the bias of the primary velocity estimate due to wind shear is obtained:

$$\Delta\tilde{V}_{lh}(\Delta S) = \begin{cases} -N\Delta S & \text{when PRF is low} \\ (N+1)\Delta S & \text{when PRF is high,} \end{cases} \quad (8)$$

where $\Delta S$ is the azimuthal shear of the radial wind component. The bias, which has been indicated in Fig. 5, gets more pronounced for higher unfolding factors. The unambiguous velocity interval of the low PRF measurement for $N = 3$ unfolding has been indicated in the figure as well. When the primary dual PRF velocity estimate is deviating more than the unambiguous velocity, the original velocity is assigned to an incorrect Nyquist interval. The fraction of incorrectly dealiased data points $\eta$, which is marked by the shaded area in Fig. 5, can be calculated using

$$\eta_i = \frac{1}{2}\left[\text{erfc}\left(\frac{V_i^u - \Delta\tilde{V}_{lh}}{\sqrt{2}\sigma_{lh}}\right) + \text{erfc}\left(\frac{V_i^u + \Delta\tilde{V}_{lh}}{\sqrt{2}\sigma_{lh}}\right)\right] \quad (9)$$

$$\eta = \frac{1}{2}[\eta_l + \eta_h], \quad (10)$$

where erfc($x$) is the complementary error function (Press et al. 1992). This equation describes the effect of both

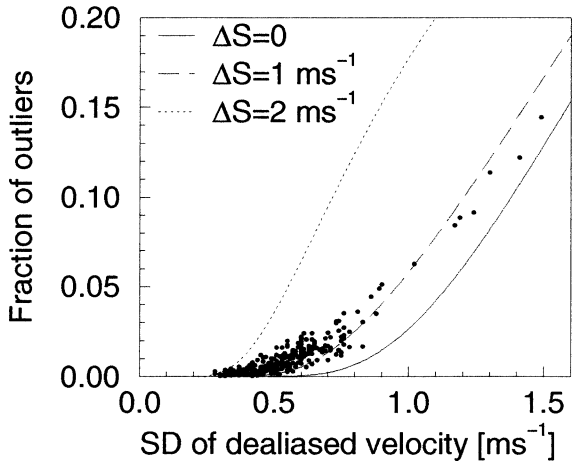


FIG. 6. Fraction of dealiasing errors as a function of the std dev of the original–dealiased velocities. About 300 different azimuthal scans (see section 3) have been used to compile this figure. In addition, three theoretical curves for azimuthal wind shears of 0, 1, and 2 m s$^{-1}$ are shown.

standard deviation and wind shear on the fraction of dealiasing errors in dual PRF velocity data.

The fraction of velocity outliers and the standard deviation of the dealiased velocities can be determined from a dual PRF Doppler azimuthal scan using the method described previously (see Fig. 2). In Fig. 6, the fraction of outliers is plotted as a function of the standard deviation of the dealiased velocities for the set of 300 azimuthal scans (see section 3). In addition, the theoretical dependence as implied by Eq. (10) is plotted for three different azimuthal shears of the radial wind. The standard deviation of the original/dealiased velocities has been converted to that of the primary dual PRF velocity estimates using the multiplication factor given by Table 1. The solid curve representing the theoretical fraction of outliers without any wind shear neatly sets the lower boundary for the experimental data. The majority of the experimental data points in Fig. 6 are grouped around the theoretical curve for an azimuthal shear of 1 m s$^{-1}$. For a typical standard deviation of 0.5 m s$^{-1}$, the fraction of dealiasing errors is on the order of 0.01. For higher unfolding factors, the number of dealiasing errors will increase dramatically due to the increase of the standard deviation of the primary velocity estimate. Equation (10) can also be utilized to quantitatively investigate the effect of changing the unfolding factor from $N = 3$ to, for instance, $N = 4$. For a typical standard deviation of $\overline{\sigma} = 0.5$ m s$^{-1}$ and a wind shear of $\Delta S = 1.5$ m s$^{-1}$, the fraction of outliers increases from 0.008 to 0.05 upon this slight increase of the unfolding factor. It will be detailed below that a certain amount of dealiasing errors can be corrected in a reliable way.

## 5. Correction of dual PRF data

From the preceding it is evident that radial velocity data obtained using the dual PRF technique cannot be fed as such to feature detection algorithms or a dual Doppler wind field analysis. In this section a three-step postprocessing algorithm is proposed that enhances the quality of the dual PRF velocity data significantly. This algorithm is intended for real-time operational use and will be implemented at KNMI in the near future. It will be shown that the quality of the dual PRF velocity data thus becomes high enough to enable all kinds of further use. The postprocessing algorithm essentially consists of the following steps.

1) *Group-size filtering.* The dual PRF velocity data are filtered based on the size and the clutter fraction of groups of connected data points.
2) *Global dealiasing.* Dealiasing of radial velocities that fall outside of the extended unambiguous velocity interval is primarily performed to ensure robustness of the algorithm, because the extended unambiguous velocity interval is usually large enough.
3) *Local dealiasing.* Using the known error characteristics of the dual PRF data, velocity outliers are corrected in an efficient way.

It should be noted that these steps have to be performed on the data in the listed order. All steps of the algorithm will be described in more detail below.

During the first step, clutter and noise are removed from the dual PRF data by filtering on group size. As a start, the rays that are blocked by nearby buildings are removed entirely from the azimuthal scan. Subsequently, a filter based on the size and clutter fraction of groups of connected data points is applied. For this, groups of connected and valid data points are labeled using an efficient algorithm described by Gonzalez and Woods (1992) and a ready algorithm for sorting labels into equivalent classes (Press et al. 1992). The labeling algorithm only looks for connections via the four closest neighbors of each data point. The periodic boundary of the polar radar data in azimuthal direction is treated properly. Then, the number of data points and ''zero velocity'' points ($V < 1.5$ m s$^{-1}$) per group of connected data points are counted. Groups consisting of less than a certain minimum number of data points are removed entirely from the azimuthal scan. In Fig. 7, the minimum number of data points per group is plotted as a function of the maximum range of the group. The minimum group size is 25 at zero range, and it gradually decreases to 10 at maximum range. The rationale behind this range dependence is the decrease of the volume represented by each data point for a shortening range. Up to a range of about 25 km, groups containing more zero velocity points than other points are removed entirely from the azimuthal scan as well. Via this group size filtering, noise from incidental scatterers at short ranges and persistent clutter due to sidelobes are removed effectively without affecting the signal at long ranges. After filtering of a scan, the minimum size of groups of connected data points is known, and this will be of advantage during the third step of the algorithm. In the remaining,

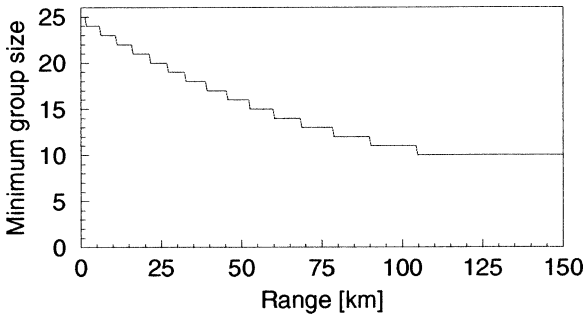


FIG. 7. Minimum required number of data points per group as a function of the maximum range of the group. This parabolic curve is characterized by the minimum group size at zero range (25) and that at maximum range (10), where the parabola has its minimum.

all valid data points will be preserved and only be corrected when needed.

The global dealiasing, which is the second step, usually has no effect on the data, but is designed to restore large-scale dealiasing errors. Velocities outside of the extended unambiguous interval, which is 40 m $s^{-1}$ in our case, cannot be dealiased correctly by the dual PRF technique. These dealiasing errors will result, just as for single PRF velocity data (Doviak and Zrnić 1993; Eilts and Smith 1990; Jing and Wiener 1993), in long boundaries of velocity discontinuities and large areas with incorrect velocity values. For dual PRF data, however, large-scale dealiasing errors are less likely to occur because of the extended unambiguous velocity interval. Numerous methods for dealiasing of single PRF data that in principle can also be applied to dual PRF data have been developed (Ray and Ziegler 1977; Merritt 1984; Desrochers 1989; Eilts and Smith 1990; Jing and Wiener 1993). Most methods rely heavily on local continuity of the wind field and use a reference wind profile (Eilts and Smith 1990) or a wind model (Merritt 1984) for dealiasing of isolated areas. Taking into account the large unambiguous interval of the dual PRF data, a rather straightforward method based on a reference wind profile is adopted. The wind profile is used to determine the proper Nyquist interval for each data point (Hennington 1981), and the velocities are dealiased by adding or subtracting $2V_{lh}^{u}(\simeq 80$ m $s^{-1})$. An upper-air sounding or a model profile can be used as the reference profile, but the use of a radar velocity azimuth display (VAD; Browning and Wexler 1968) or volume velocity processing (VVP; Waldteufel and Corbin 1979) profile is preferred. These radar wind profiles are based on a linear wind model and are by definition available at the radar site. Aliasing errors are generally no problem in these profiles, because of differences in measurement strategy and corrections made by the profile algorithms. This step is implemented as a safety because the third step cannot handle large-scale dealiasing errors.

During the third and final step, local dealiasing errors are corrected using the known error characteristics of dual PRF data. It has been detailed in section 4 that these outliers can be identified by their deviation from the local median velocity. The calculation of the local median velocity is based on at least nine valid data points. In first instance the nine data points are sought in the $3 \times 3$ square centered at the data point. When not enough valid data points are present in this square, the square is enlarged step by step until the required number of points is collected. The ''adaptive'' local median velocity can be determined for each data point, since the minimum number of connected points per group is known from the group size filtering of the first step. Data points deviating more than the unambiguous velocity from the local median velocity are considered as outliers. For both the detection and correction of the outliers, it is crucial that the PRF (high or low) and thus the unambiguous velocity is known for each ray. This information can be obtained from the histogram analysis presented in Fig. 2, but it should be extracted from the radar processor to ensure operational robustness. The deviation of the outliers from the local median velocity is minimized by adding or subtracting multiples of twice the appropriate unambiguous velocity. By correcting the outliers in this way, the spatial resolution of the velocity data is retained and no smoothing of any kind is applied. In addition, this correction method is very efficient because the local median velocity is determined from nine valid data points thus allowing up to four nearby outliers. Several passes of the local dealiasing algorithm may be required when the local concentration of outliers is high, for instance in areas with a high wind shear or a large spectral width.

The improvements provided by the three-step postprocessing algorithm are illustrated by two examples in Fig. 8. The upper frames of this figure show the raw and processed velocity data obtained during the passage of a cold front. This case is also shown in Fig. 1 and details have been given in section 4. It is evident that the raw velocity data in Fig. 8a of the figure contain numerous deliasing errors. The velocity data after the group size filtering and a single pass of the local deliasing algorithm are shown in Fig. 8b. Application of the global dealiasing step is not needed because the wind speed is well below the extended unambiguous velocity. For these long ranges and large groups of connected data points, the group size filtering has hardly any effect. The first pass of the local dealiasing algorithm effectively corrects the outliers. Two remaining outliers in the upper-right corner are corrected after a second pass. Velocity data obtained from showers in past-frontal cold air are shown in Figs. 8c,d. Some of these showers produced hail and/or severe wind gusts up to 28 m $s^{-1}$. The raw velocity data shown in Fig. 8c are clearly contaminated by noise, sidelobe clutter, and outliers. Figure 8d shows the velocity data after group size filtering and a single pass of the local dealiasing algorithm. At this short range, the group size filter removes noise and clutter without effecting the main structures. All velocity

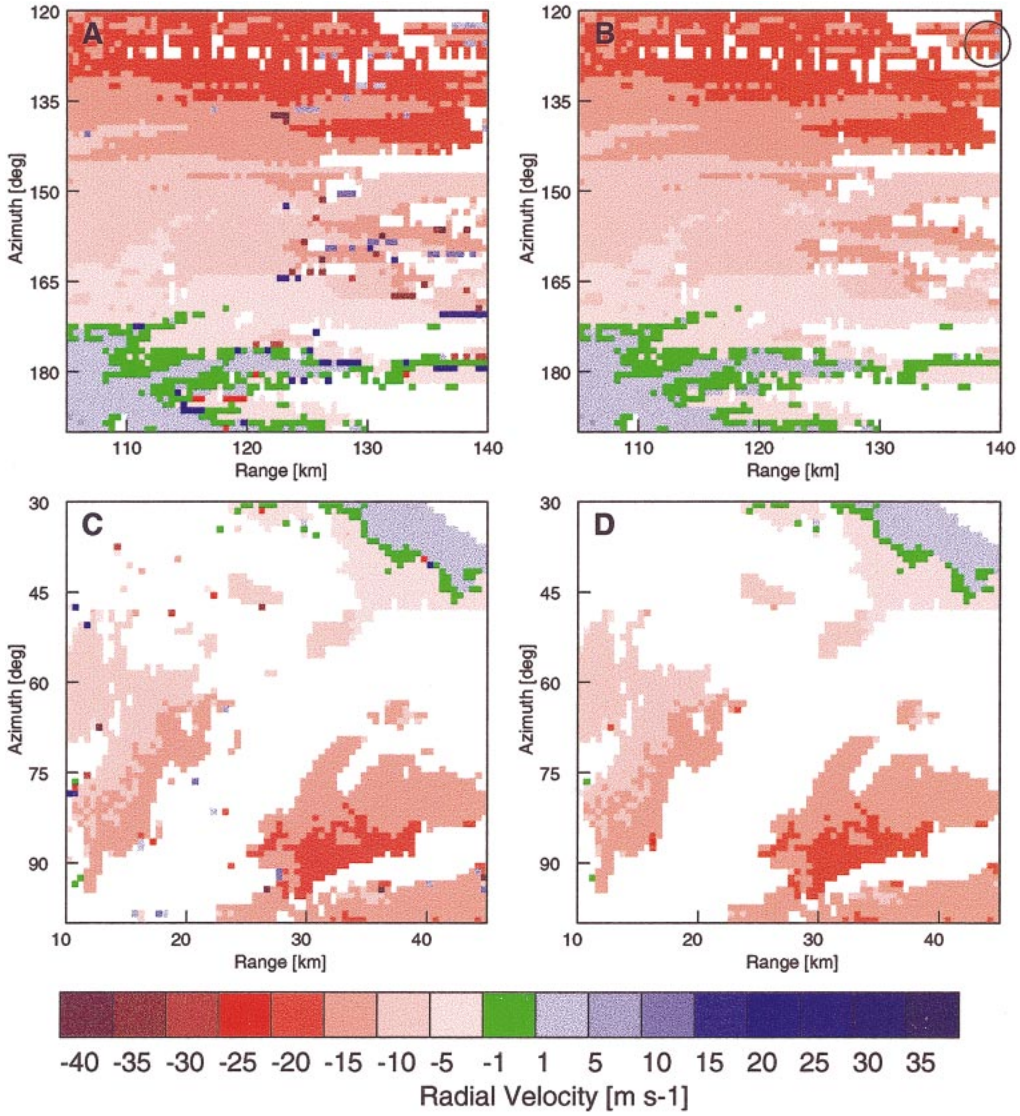


FIG. 8. Two examples of raw and processed dual PRF velocity data. (a), (d) Velocity data from 1454 UTC 6 Nov 2001: (a) also shown in Fig. 1; (b) the processed data. (c), (d) Velocity data from 1054 UTC 22 Nov 2001. The raw and processed data are shown in (c) and (d), respectively. In both cases, group size filtering and a single pass of the local dealiasing algorithm have been applied. Two remaining outliers in (b) are marked.

outliers are corrected by a single pass of the local dealiasing algorithm.

Preliminary results on the performance of the postprocessing algorithm have been obtained. The algorithm has been applied to the set of 300 azimuthal scans (see section 3). During the processing of the scans, the average fraction of outliers and the percentage of high-quality scans have been monitored. Azimuthal scans with a fraction of outliers $\eta$ smaller than 0.001 are defined to be of ''high quality'' in this study. The results for the raw scans, the group size filtered scans, and the corrected scans after one, two, and three pass(es) of local dealiasing algorithm are listed in Table 2. The global dealiasing step has been skipped because the maximum wind speed in the set of azimuthal scans is considerably lower than the extended unambiguous velocity. The averaged outlier fraction of the untreated scans is roughly 0.01 and the percentage of high quality scans is only 3.5%. On average, about 7% of the data points are removed by group size filtering of the azimuthal scans. The first pass of the local dealiasing algorithm decreases the average fraction of outliers by a factor of 25 and increases the percentage of high quality scans to roughly 90%. After the second pass, the percentage of high quality scans is already approaching 100%. So high quality velocity data are usually obtained by application of the postprocessing algorithm with only a single pass of the local dealiasing algorithm.

TABLE 2. Results of the application of the three-step postprocessing algorithm on the set of 300 azimuthal scans (see section 3). The average fraction of outliers $\bar{\eta}$ and the percentage of high quality scans, that is, with a fraction of outliers $\eta < 0.001$, are considered. The results for the raw scans, the group size filtered scans, and the corrected scans after one, two, and three pass(es) of local dealiasing algorithm are listed.

| | Raw | Filter | First pass | Second pass | Third pass |
|---|---|---|---|---|---|
| $\bar{\eta}$ | 0.011 | 0.010 | $3.9 \times 10^{-4}$ | $1.1 \times 10^{-4}$ | $6.3 \times 10^{-5}$ |
| $\eta \leq 0.001$ | 3.5% | 4.2% | 89.5% | 99.3% | 99.7% |

## 6. Conclusions

Fields of radial velocity data obtained using the dual PRF technique have been analyzed quantitatively. The standard deviation of the velocity estimates and the fraction of dealiasing errors are extracted. In addition, the positions of the outlier sidebands as observed for rays with even and odd azimuths can be used to assign the proper PRF to each ray. It is shown experimentally that the standard deviation of the velocity estimates depends on the spectral width and thus on the meteorological circumstances. A simple model has been employed to describe the dependence of the fraction of dealiasing errors on the standard deviation of the velocity estimates and the azimuthal shear of the radial wind. Quantitative agreement between the observed and modeled fraction of dealiasing errors as a function of the standard deviation is found.

A three-step postprocessing algorithm for enhancing the quality, and thus the employability, of dual PRF velocity data has been developed. The postprocessing algorithm, which removes noise and corrects dealiasing errors, is intended for operational use. The spatial resolution of the velocity data is retained, however, because no smoothing is performed. Preliminary results on the performance of the algorithm have been obtained by the processing of about 300 azimuthal scans. It is found that high quality dual PRF velocity data, that is, scans with a fraction of outliers smaller than 0.001, are produced routinely using the three-step algorithm. The majority of the azimuthal scans (90%) are upgraded to high quality by the group size filtering and a single pass of the local dealiasing algorithm, while for the remaining ones, only two or three passes are needed. In conclusion, the postprocessing algorithm is very efficient and produces dual PRF velocity data of high quality. Bird migration and ground clutter may still cause problems in the processed dual PRF velocity data, just as they would in single PRF data. The postprocessing algorithm for dual PRF data will be implemented at KNMI, and this will enable further development of Doppler radar applications, like detection of wind shear, dual Doppler wind fields, and assimilation into NWP models.

*Acknowledgments.* Herman Wessels and Sylvia Barlag are gratefully acknowledged for their support and careful reading of the manuscript.

REFERENCES

Bergen, W. R., and S. C. Albers, 1988: Two- and three-dimensional de-aliasing of Doppler radar velocities. *J. Atmos. Oceanic Technol.,* **5,** 305–319.

Bluestein, H. B., and A. L. Pazmany, 2000: Observations of tornadoes and other convective phenomena with a mobile, 3-mm wavelength, Doppler radar: The spring 1999 field experiment. *Bull. Amer. Meteor. Soc.,* **81,** 2939–2951.

Browning, K. A., and R. Wexler, 1968: The determination of kinematic properties of a wind field using Doppler radar. *J. Appl. Meteor.,* **7,** 105–113.

Chong, M., and Coauthors, 2000: Real-time wind synthesis from Doppler radar observations during the Mesoscale Alpine Programme. *Bull. Amer. Meteor. Soc.,* **81,** 2953–2962.

Collins, W. G., 2001: The quality control of velocity azimuth display (VAD) winds at the National Centers for Environmental Prediction. Preprints, *11th Symp. on Meteorological Observations and Instrumentation,* Albuquerque, NM, Amer. Meteor. Soc., 317–320.

Dazhang, T., S. G. Geotis, R. E. Passarelli Jr., A. L. Hansen, and C. L. Frush, 1984: Evaluation of an alternating-PRF method for extending the range of unambiguous Doppler velocity. Preprints, *22d Conf. on Radar Meteorology,* Zurich, Switzerland, Amer. Meteor. Soc., 523–527.

Desrochers, P. R., 1989: A reliable method for real-time velocity unfolding. Preprints, *24th Conf. on Radar Meteorology,* Tallahassee, FL, Amer. Meteor. Soc., 415–418.

Doviak, R. J., and D. Sirmans, 1973: Doppler radar with polarization diversity. *J. Atmos. Sci.,* **30,** 737–738.

——, and D. S. Zrnić, 1993: *Doppler Radar and Weather Observations.* 2d ed. Academic Press, 562 pp.

Eilts, M. D., and S. D. Smith, 1990: Efficient dealiasing of Doppler velocities using local environment constraints. *J. Atmos. Oceanic Technol.,* **7,** 118–128.

Gonzalez, R. C., and R. E. Woods, 1992: *Digital Image Processing.* Addison-Wesley, 716 pp.

Hennington, L., 1981: Reducing the effects of Doppler radar ambiguities. *J. Appl. Meteor.,* **20,** 1543–1546.

Hildebrand, P. H., and Coauthors, 1996: The ELDORA/ASTRAIA airborne Doppler weather radar: High-resolution observations from TOGA COARE. *Bull. Amer. Meteor. Soc.,* **77,** 213–232.

Hondl, K. D., and M. D. Eilts, 1993: Evaluation of Doppler velocity dealiasing techniques for low-Nyquist velocity data. Preprints, *26th Conf. on Radar Meteorology,* Norman, OK, Amer. Meteor. Soc., 59–61.

Jing, Z., and G. Wiener, 1993: Two-dimensional dealiasing of Doppler velocities. *J. Atmos. Oceanic Technol.,* **10,** 798–808.

Jorgensen, D. P., T. R. Shepherd, and A. S. Goldstein, 2000: A dual-pulse repetition frequency scheme for mitigating velocity ambiguities of the NOAA P-3 airborne Doppler radar. *J. Atmos. Oceanic Technol.,* **17,** 585–594.

Lindskog, M., H. Järvinen, and D. B. Michelson, 2000: Assimilation of radar radial wind in the HIRLAM 3D-Var. *Phys. Chem. Earth B,* **25,** 1243–1250.

May, P. T., 2001: Mesocyclone and microburst signature distortion with dual PRT radars. *J. Atmos. Oceanic Technol.,* **18,** 1229–1233.

——, and P. Joe, 2001: The production of high quality Doppler velocity fields for dual PRT weather radar. Preprints, *30th Conf. on Radar Meteorology*, Munich, Germany, Amer. Meteor. Soc., 286–288.

Meischner, P., C. Collier, A. Illingworth, J. Joss, and W. Randeu, 1997: Advanced weather radar systems in Europe: The COST 75 action. *Bull. Amer. Meteor. Soc.*, **78,** 1411–1430.

Merritt, M. W., 1984: Automatic velocity de-aliasing for real-time applications. Preprints, *22d Conf. on Radar Meteorology*, Zurich, Switzerland, Amer. Meteor. Soc., 528–533.

Press, W. H., S. A. Teukolsky, W. T. Vetterling, and B. P. Flannery, 1992: *Numerical Recipes in C: The Art of Scientific Computing.* 2d ed. Cambridge University Press, 994 pp.

Ray, P. S., and C. Ziegler, 1977: De-aliasing first-moment Doppler estimates. *J. Appl. Meteor.,* **16,** 563–564.

Sachidananda, M., and D. S. Zrinć, 2000: Clutter filtering and spectral moment estimation for Doppler weather radars using staggered pulse repetition time (PRT). *J. Atmos. Oceanic Technol.,* **17,** 323–331.

Serafin, R. J., and J. W. Wilson, 2000: Operational weather radar in the United States: Progress and opportunity. *Bull. Amer. Meteor. Soc.,* **81,** 501–518.

SIGMET, 1998: RVP6 Doppler signal processor user's manual. Sigmet, Westford, MA, 204 pp.

Sirmans, D., D. Zrnić, and B. Bumgarner, 1976: Extension of maximum unambiguous Doppler velocity by use of two sampling rates. Preprints, *17th Conf. on Radar Meteorology*, Seattle, WA, Amer. Meteor. Soc., 23–28.

Waldteufel, P., and H. Corbin, 1979: On the analysis of single-Doppler radar data. *J. Appl. Meteor.,* **18,** 532–542.